Original article

JOURNAL OF REINFORCED PLASTICS & COMPOSITES

Journal of Reinforced Plastics and Composites
2018, Vol. 37(3) 181–190

DOI: 10.1177/0731684417738335
journals.sagepub.com/home/jrp
SAGE

Boracic polyethylene/polyethylene wax blends and open-cell nickel foams as neutron-shielding composite

Yun Zhang[1], Feida Chen[1], Xiaobin Tang[1,2], Hai Huang[1], Tuo Chen[1] and Xiangyu Sun[1]

Abstract

This work shows that mechanical properties, thermal conductivity, and secondary gamma-ray shielding ability can be significantly improved when open-cell nickel foams are embedded into the shielding composites. The boracic polyethylene/polyethylene wax blends and open-cell nickel foam composites (PPNM) are designed and prepared by permeating homogeneous mixed melt fillers into open-cell nickel foams. The ratio of polyethylene and polyethylene wax is investigated to achieve higher filling rate. The quasi-static compressive response of PPNMs and polyethylene/polyethylene wax blends is measured, and the crystallization properties are studied by differential scanning calorimetry. The neutron and secondary gamma-ray shielding abilities of PPNMs are also simulated based on Monte Carlo particle transport method. Results show that the compression strength of PPNMs with boron carbide is slightly improved when compared with polyethylene/polyethylene wax blends. The nickel foams in PPNM composites improve the energy-absorbing efficiency by 30%. The thermal conductivity of PPNMs is 300% higher than polyethylene/polyethylene wax. The calculated results show that neutron-shielding abilities of PPNMs increase as content of boron carbide increases. Moreover, secondary gamma-ray shielding ability of PPNMs containing boron carbide is obviously higher than polyethylene/polyethylene wax. The PPNMs containing boron carbide neutron-shielding materials are proved to have good thermal conductivity, mechanical properties, and radiation-shielding ability.

Keywords

Polyethylene, nickel foams, neutron shielding, composites, compression performance, secondary gamma-rays

Introduction

Neutron-shielding materials are an important infrastructure component in many nuclear facilities for radiation protection, for example, an Am–Be source, a neutron spectrometry system, nuclear reactor, and nuclear fuel transportation casks.[1–5] They have to withstand a lengthy period in a rather inclement environment with intense neutron levels. For many nuclear facilities in more aggressive environments, advance shielding materials with excellent physical and mechanical performances could guarantee their safety, compliance, and efficiency.[6–11] The thermal conductivity is also a rather important issue because the rapid release of heat originating from nuclear reactions can ensure the safety of the system.[12,13] Owing to the limits of space and maneuverability, the researchers found that the weight and the volume of radiation-shielding material are also fairly restricted.[2] For these reasons, the neutron shield materials require high-performance composite materials with multiple properties such as mechanical properties, high thermal conductivity, low specific weight, and high general shielding properties. However, conventional neutron-shielding materials such as polymer and polymer matrix composite (i.e. polyethylene (PE), paraffin, water, boracic polyethylene, and concrete) do not meet these requirements.[14,15]

A feasible solution for modern neutron-shielding materials might be open-cell metal foams-based composites filled with polymer and functional fillers. Open-cell

[1]Department of Nuclear Science & Engineering, Nanjing University of Aeronautics and Astronautics, Nanjing, China
[2]Jiangsu Key Laboratory of Nuclear Energy Equipment Materials Engineering, Nanjing University of Aeronautics and Astronautics, Nanjing, China

Corresponding author:
Xiaobin Tang, Jiangsu Key Laboratory of Nuclear Energy Equipment Materials Engineering, Nanjing 210016, China.
Email: tangxiaobin@nuaa.edu.cn

foamed metals have gained increasing attention as a new kind of structural and functional material that possesses many fascinating properties,[16–18] including high specific strength, low density, high energy absorption capacity, etc.[19,20] It is a porous structure with an interconnected three-dimensional (3D) metallic skeleton.[21] Recently, the research by Chen et al., provided useful insight on the correlation of neutron-shielding effectiveness with metal foam structure.[22,23] Owing to the properties of strong erosion resistance, high thermal conduction, and mechanical strength, foamed nickel was assumed to effectively enhance the comprehensive radiation-shielding ability, energy absorption efficiency, and thermal conductivity of polymer-based composite materials. In addition, PE is an outstanding neutron moderating material known for its high hydrogen content. Therefore, the PE/nickel foam metal composites should be promising new neutron-shielding materials.

However, the production of this material is still problematic. This type of metal porous polymer composite is normally produced by infiltrating polymers into a porous metal structure.[18,24,25] Infiltrating requires much lower viscosity of polymer melt than that of PE to achieve high filling rate and strength. Moreover, addition of neutron-rich materials (i.e. B_4C and BN_m) to PE is often needed to achieve higher neutron-absorbing efficiency, which increases the melt viscosity. In this study, we prepared a new boracic PE/polyethylene wax (PEW) blends–open-cell nickel foam composites (PPNMs) by the penetration method. PEW was used to reduce the viscosity of PE. The preparation processing was studied for the high filling rate, homogeneity of boron carbide, and interface banding. The neutron-shielding effectiveness of this composite was explored by using the Monte Carlo Particle Transport simulation method.

Materials and methods

Materials and sample preparation

The PPNM composites were prepared by surface treatment, uniform mixing, fusion, and filtration filling under negative pressure. First, open-cell foamed nickel (relative density: 0.05, cell density: 6 PPI) was prepared in suitable size and pretreated in petroleum ether and dilute hydrochloric acid solution to remove oil and oxide on the surface. Carbide boron and nickel foams were surface treated by 5 wt.% trimethoxyvinylsilane (K-151, Huaian Heyuan Chemical Co., Ltd.). Second, the carbide boron, PEW, and PE were mixed using a magnetic stirrer for 15 min. Finally, the mixed powder was melted at 170°C and filtered into nickel metal at a negative pressure. The surplus polymer captured by the surface of the composite was carefully removed. The carbide boron had an average particle size of 5 μm (China Jilin Dunhua Zhengxing Abrasive Co., Ltd.). The PE and PEW have an average particle size of 70 μm (Thailand SCG). The detailed constituent content of specimens is shown in Table 1.

Table 1. Composition and density information of PPNM composites.

Sample classification	Composition information (mass fraction of B_4C in fillers)	Density of composites (g/cm)
PE/PEW	PE (50%), PEW (50%)	1.01
PPNM–0% B_4C	PE (50%), PEW (50%)	1.26
PPNM–10% B_4C	PE (45%), PEW (45%), B_4C (10%)	1.31
PPNM–20% B_4C	PE (40%), PEW (40%), B_4C (20%)	1.39
PPNM–30% B_4C	PE (35%), PEW (35%), B_4C (30%)	1.48
PPNM–40% B_4C	PE (30%), PEW (30%), B_4C (40%)	1.56

Characterization and computational methods

The viscosity of the system was measured with an NDJ-1 rotary viscosity meter at 160°C. A scanning electron microscope (SEM, JSM-750, JEOL) was used to observe the fracture surface morphology of boracic PE/PEW. An optical microscope (WTL-17AT) was performed to confirm the quality of the filling process. The thermal properties of fillers were determined by a using differential scanning calorimeter (DSC Q20 V24.11) with nitrogen as purge gas and a heating rate of 20°C/min. Compression examinations were performed using an WANCE ETM-105D system according to ISO 13314-2011. The rate of compression was 1.2 mm/min. Grease was applied to the compression platen surface that would press against the specimen. Thermal conductivity was determined using a DRL thermal conductivity test system. Composite specimens with dimensions of 20 mm × 20 mm × 10 mm were used. The test result obtained from three measurements was used to minimize errors in the effective thermal conductivity experiment.

The simulation of neutron shielding was performed by Monte Carlo N-Particle Transport Code version 5 (MCNP5), which was developed by the Los Alamos National Laboratory. The MCNP code is based on the Monte Carlo method, which can realistically describe random events and calculate the particle transport problem.[26] Given that the problem is dealing with neutron and secondary photon interaction with the desired sample, MCNP code runs in neutron and photon mode. The schematic diagram of model is shown in Figure 1(a). A isotropic point source was placed at the center of the spherical shell-shaped shield. A spherical detector was set for dose detection.

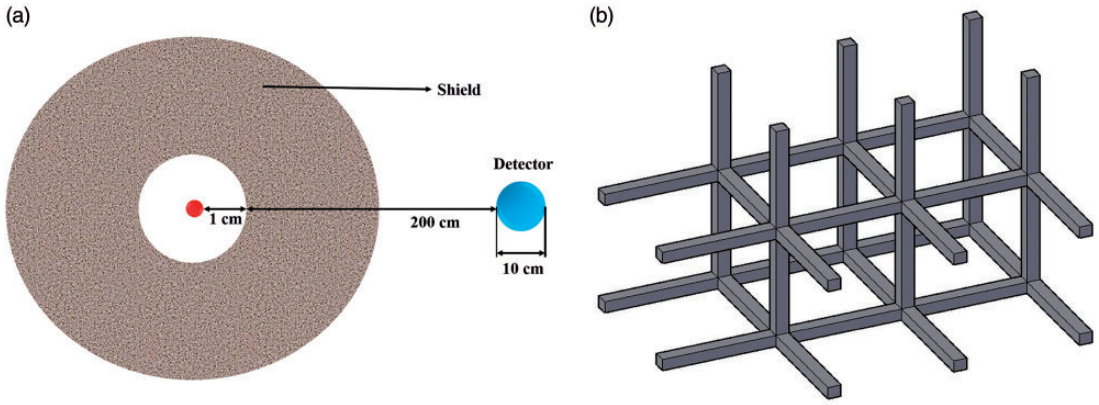

Figure 1. The schematic diagram of model for MCNP simulation (a) whole geometrical model, (b) open-cell nickel foam model.

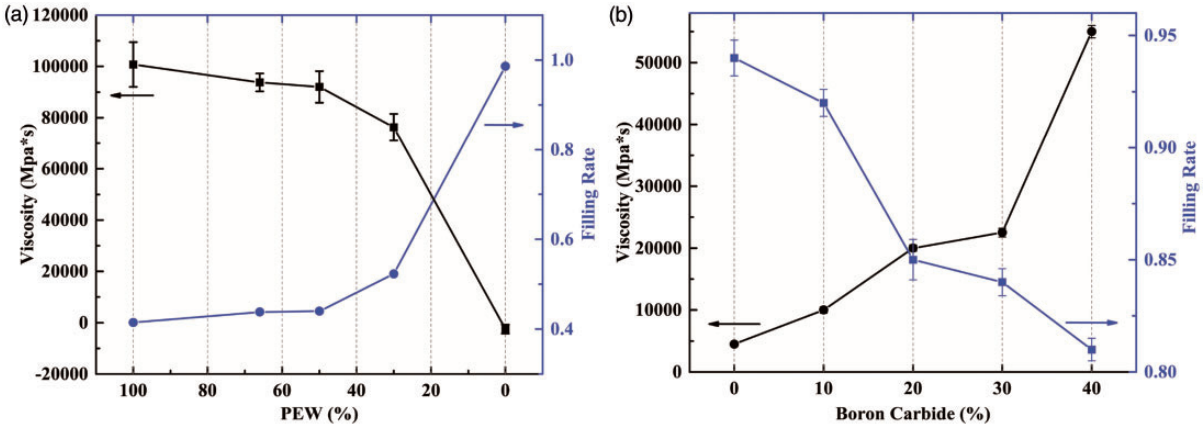

Figure 2. The influence of (a) the content of PEW on the viscosity of melt and filling rate, (b) the content of boron carbide on the viscosity of melt and filling rate.

Pure water was defined for inside of detector. F4 tally (flux over detector cell) was concerned with the total cross-section.[27] DE and DF cards were used to convert flux to dose. All the data obtained by MCNP5 were reported with less than 1% error.

Owing to the geometrical complexity and random orientation of the solid phase of the porous medium, the researchers found that the real geometry of foams is unpractical for modeling unless geometric idealization is employed by using a periodic unit cell.[10,23] Figure 1(b) shows the simplified 3D microstructure of the open-cell nickel foam model developed in this study. The consistency of the simulation and experiment result was proved in previous work.[28]

Results and discussion

Viscosity and filling rate

Figure 2 shows the viscosity of the melt and the filling rate of the PPNM–0% B_4C composite with various PE contents. When the content of PE was higher than 50%, the viscosity of melt and the filling rate of nickel foams obviously increased. Figure 3 displays the typical macroscopic picture of the cross-section of the PPNM composites with different filling rates. The samples in Figure 3(a) to (c) have a ratio of 1:1 between PE and PEW. The sample in Figure 3(d) has a ratio of 2:1 between PE and PEW, and many unfilled cell in nickel foams were found. Therefore, a 1:1 relationship between PE and PEW was chosen for the PPNM composites. Figure 2(b) shows the viscosity of the melt and the filling rate of the PPNM composites with various B_4C contents. The B_4C content in the range of 0–40% also obviously increased melt viscosity, whereas the filling rate was higher than 80%. The photomicrograph of the PPNM composites cross-section is shown in Figure 4. No obvious interfacial voids are found at the interface between nickel and fillers. The fillers melt exhibited a good wettability on nickel foam after surface treatment.

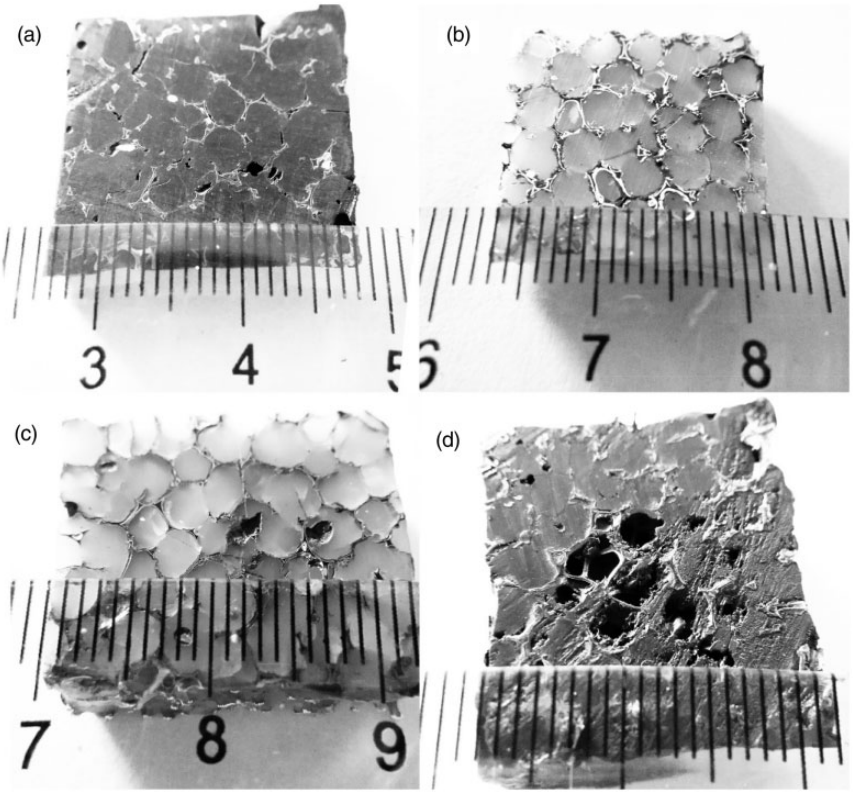

Figure 3. Picture of the cross-section of the PPNM composite with different filling rate (a) 90%, (b) 95%, (c) 86%, and (d) 40%.

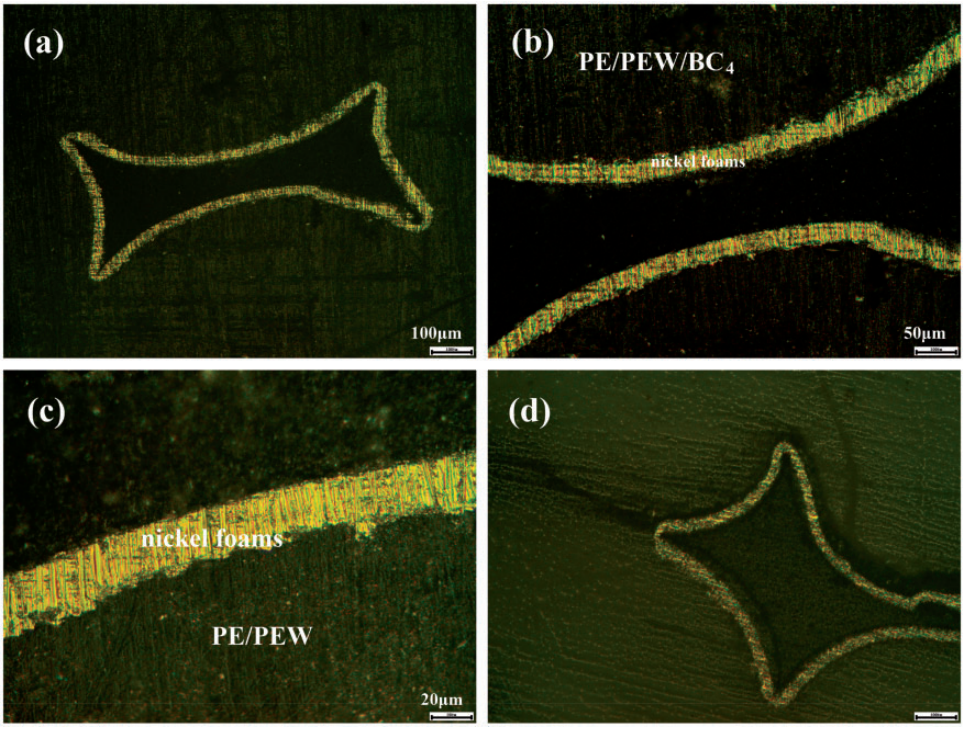

Figure 4. OM photomicrograph of cross section of the PPNM composite (a) 20% B_4C, (b) a magnified image of (a), (c) 0% B_4C, and (d) 40% B_4C.

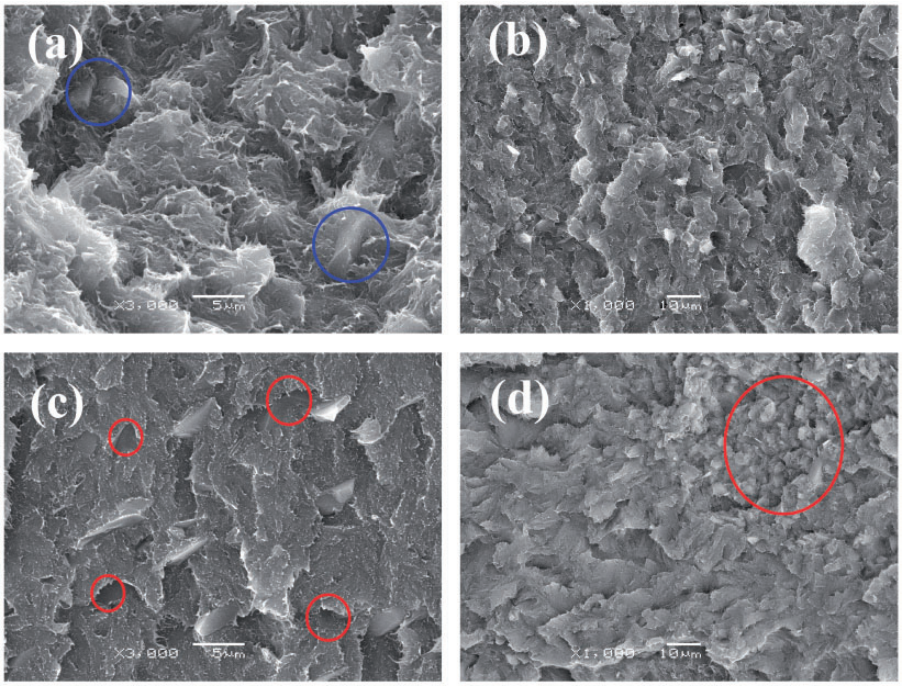

Figure 5. SEM micrographs of the fractured surface of Boracic PE/PEW Blends: (a) 20% B4C with surface treatment, (b) a magnified image of (a), (c) 20% B_4C without surface treatment, and (d) a magnified image of (c).

Morphology observation

The surface treatment of B_4C affected the morphology of boracic PE/PEW blends and the adhesion between PE/PEW Blends matrix and B_4C particles. Figure 5(a) and (b) displays the SEM micrograph of the fracture surface and the composite containing B_4C with surface treatment. The B_4C particles exhibited a good dispersion in the matrix without interfacial voids and obvious desquamate of particles. In Figure 5(c), the desquamate of some B_4C particles without surface treatment was formed during the fracture. As shown in Figure 5(d), the agglomeration of particles was observed in boracic PE/PEW blends without surface treatment. Hence, the surface treatment in this work is effective and necessary.

Effective thermal conductivity

The effective thermal conductivities of PE/PEW blends–open-cell nickel foams composite and PE/PEW blends are listed in Table 2. The neat PE has an effective thermal conductivity of 0.50 W/m K. The addition of PEW slightly increased thermal conductivity. The PPNM–0% B_4C composite showed a much higher thermal conductivity than PE/PEW. The nickel foams account for just 5% of the composite, but the 3D metal network vastly enhanced heat flow.

Table 2. Thermal conductivity test result.

Sample	Hot face (°C)	Cold face (°C)	Heat flux (W)	Heat resistance (°C × cm^2/W)	Heat conductivity coefficient (W/mK)	Error (%)
PPNM	61.258	26.880	3.143	37.19	2.4200	0.43
PEW/PE	62.422	26.618	0.893	144.34	0.6235	0.06

The compressive performance

Figure 6(a) shows the stress–strain curves of nickel foams without fillers. The curves of the compression of the nickel foams comprise of two regions, namely elastic deformation and plastic deformation (plateau region).[29,30] In the elastic deformation region, a sharp increase in stress which at first sight was observed to be linear for a small strain in compression.[31] The plateau region of nickel foams in this work shows fluctuation in the range of 1.3–1.9 MPa, which means that localized crush and deformation spread to the rest of the specimen as the compression test progressed. The densification is not obvious till the strain reached 0.5.

For the PE/PEW, the typical fast failure pattern occurred when the strain reached 0.15, as shown in Figure 6(b). The PE/PEW blends were quickly crushed into debris during the compressive process. The compressive stress vs. strain response for five types of

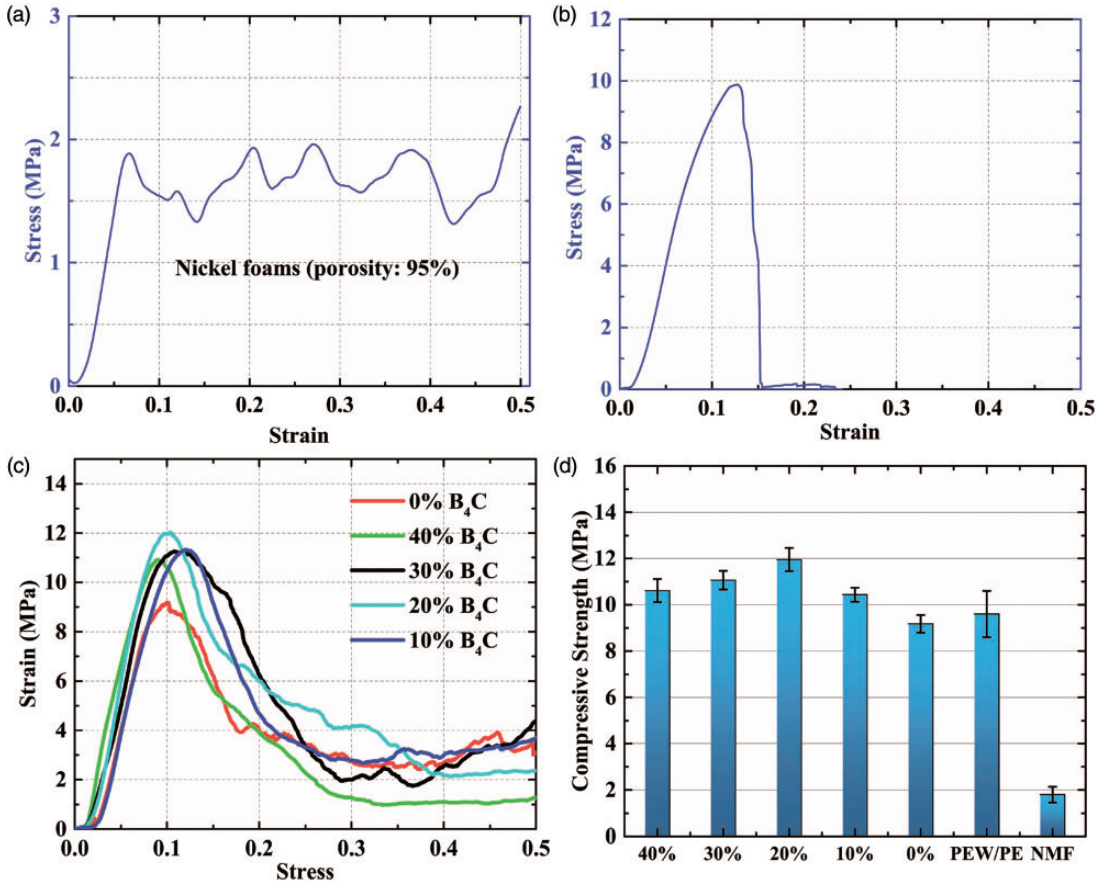

Figure 6. (a) Stress–strain curves of nickel foams, (b) stress and strain curves of PE/PEW, (c) stress and strain curves of PPNM composite, and (d) compressive strength.

PPNM composites are shown in Figure 6(c). These responses show three stages of deformation. An initial linear elastic region is followed by a slower and wider drop than that of PE/PEW in stress with increasing strain after yielding. The softening response is then followed by a plateau region of small moving stress with increasing strain. The plateau stress is slightly higher than that of nickel foams.[16] Moreover, Figure 6(d) shows the compressive strength of nickel foams, FE/FEW blends, and PPNM composites with various filler contents. The compressive strength of the PPNM composites in this study was significantly higher than nickel foams, but almost identical with that of PE/PEW blends. PE and PEW are both semi-crystalline polymers and a considerable thermal expansion coefficient difference between blends and nickel foams was found. Solidification shrinkage of fillers cause hot cracking and stresses concentrated between nickel foams and fillers unavoidably existed in composites. All these results in the nickel foam failed in improving the compressive strength of PPNM composite. Comparing with PPNM–0% B_4C, the researchers found that the addition of B_4C fillers increased the compressive strength of PPNM. B_4C reinforced particles and reduced solidification shrinkage of fillers. On the other hand, many B_4C introduced defects into the composite, therefore the compressive strength slightly decreases from 20% to 40%.

The energy absorption efficiency, W_e is calculated using the equation below:

$$W = \frac{1}{100}\int_0^{e_0} \sigma de \tag{1}$$

$$W_e = \frac{W}{e_0 \times \sigma_0} \times 10^4 \tag{2}$$

W is the energy absorption per unit volume (MJ/m^3), W_e is the energy absorption efficiency (%), σ is the compressive stress (N/mm^2), e_0 is the upper limit of the compressive strain (%), and σ_0 is the compressive stress at the upper limit of the compressive strain (N/mm^2). Table 3 shows the energy absorption efficiency of nickel foams, PE/PEW, and the PPNM composite. W_e of the PPNM composites is almost twice that of PE/PEW but below that of nickel foams. Nickel foams

Table 3. Energy absorption efficiency.

Materials	PPNM–10% B_4C	PPNM–20% B_4C	PPNM–30% B_4C	PPNM–40% B_4C	PPNM–0% B_4C	PEW/PE	NMF
Energy absorption efficiency (%)	58.24	56.49	58.00	59.03	52.24	27.64	77.52

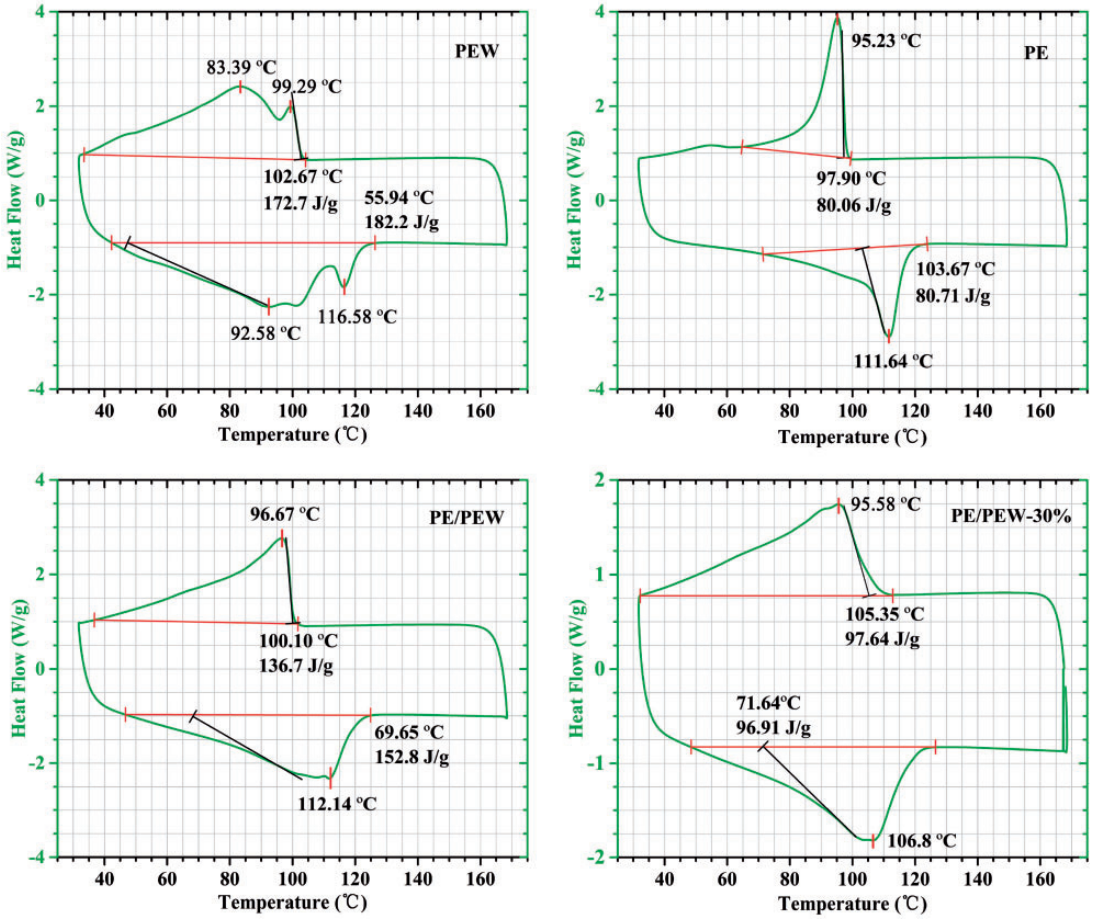

Figure 7. The DSC test result of PE, PEW, PE/PEW, and PE/PEW–30% B_4C.

increased the energy absorption efficiency of polymer blends.

Thermal property of fillers

To understand the failure of PPNMs with or without B_4C particles, the thermal behaviors of fillers were studied by DSC.[14] Figure 7 shows the second DSC curves of PE, PEW, PE/PEW, and PE/PEW–30% B_4C. The melting points (T_m), crystallizing temperature (T_c), and heat values are shown in Table 4. All the four materials are semi-crystalline materials, which result in high thermal shrinkage, stress concentration, and cracks. The heat value (ΔH_c) of PE/PEW for cooling processes was 10 J/g higher than the mean value of PE and PEW. Moreover, the double melting peak and crystallizing peak of PEW are wide, thus the molecular weight distribution is wide. The small molecular weight PEW increased segment movement of PE, which

Table 4. DSC data for the PE, PEW, PE/PEW, and PE/PEW–30% B_4C.

Sample	T_c (°C)	ΔH_c (J/g)	T_m (°C)	ΔH_m (J/g)
PEW	83.89, 99.29	172.7	92.58, 116.58	182.2
PE	95.23	80.06	111.64	80.71
PE/PEW	96.67	136.7	112.14	152.8
PE/PEW–30% B_4C	95.58	97.64	106.8	96.91

promoted the crystallization of PE/PEW, and increased the cracking and stress concentration. Thus, the compression strength of PPNM–0% B_4C was much lower than that of PE/PEW. The ΔH_c of PE/PEW–30% B_4C is approximately 70% that of PE/PEW. Therefore, the B_4C did not change the degree of crystallization, decreasing the heat shrinkage of composites. On the other hand, the start of the crystallization temperature of PE/PEW–30% B_4C is higher than PE/PEW, but the crystallization velocity was much lower than the other three samples. The B_4C plays a promoting role in nucleation site and inhibits grain growth. The surface treatment of B_4C was proved to be efficient and successfully reinforced the interface wettability between polymer and particles in this respect.

The simulation of neutron shielding

A frequently used Am–Be source energy spectrum was selected in simulations of this study, as shown in Figure 8(a). The elemental composite of fillers is listed in Table 5. The neutron dose rate of samples is shown in Figure 8(b), the result showed that the dose rate and decrease with increasing of thickness. The composites with higher B_4C content obviously obtained a lower neutron dose rate. Secondary gamma-rays are unavoidable during neutron shielding. The factor influencing the dose rate of the secondary gamma-ray in detector included the energy, number of generated photon, and the photon-shielding ability. As shown in Figure 8(c), the calculated photon dose rate of the PPNM and PE initially increased and then decreased at different thicknesses. For PPNM–10% B_4C, PPNM–20% B_4C, PPNM–30% B_4C, and PPNM–40% B_4C, when the

Table 5. Elemental composition of fillers.

Fillers	Density (g/cm^3)	Elemental composite (wt.%)
PE	0.94	H(14.29), C(85.71)
10%	1.06	H(12.85), C(79.31), B(7.2)
20%	1.22	H(11.42), C(72.91), B(15.63)
30%	1.38	H(9.99), C(66.52), B(23.37)
40%	1.58	H(8.56), C(60.12), B(31.64)

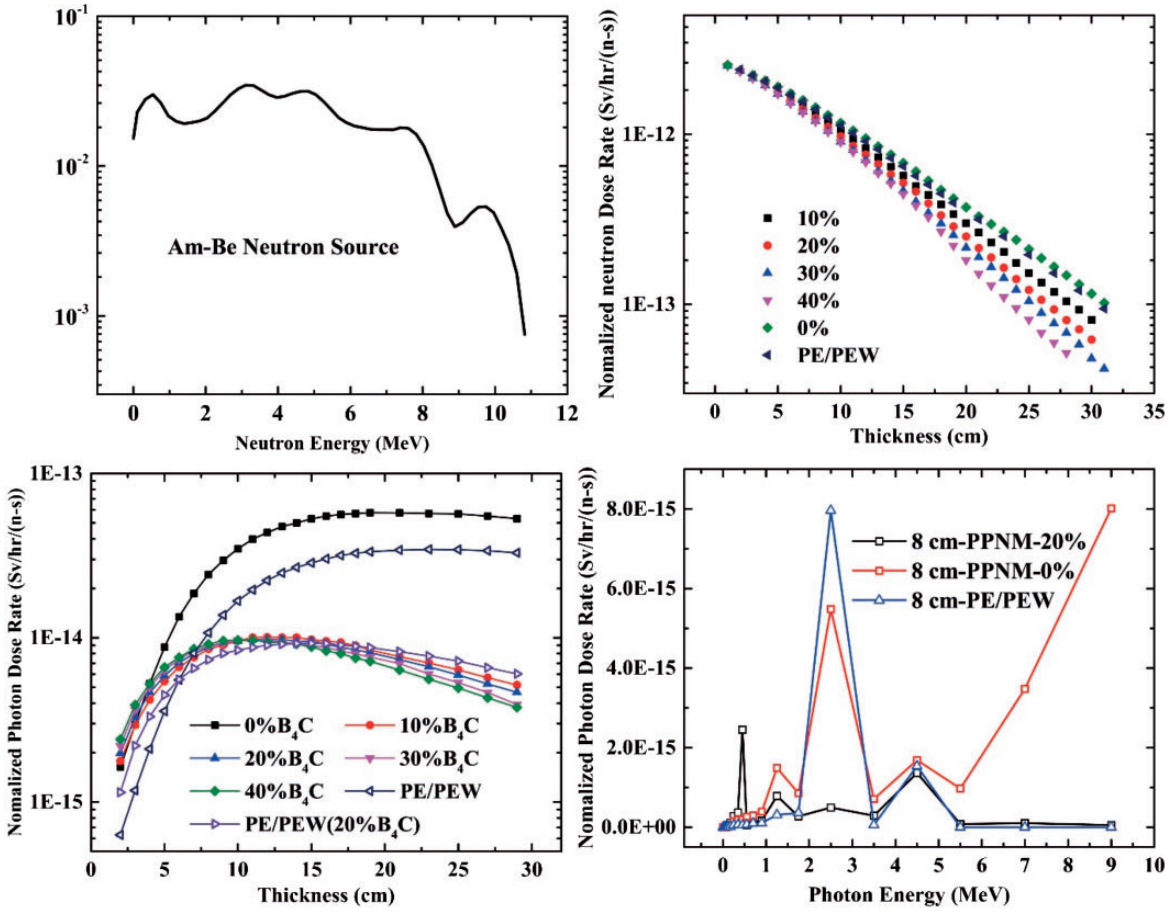

Figure 8. (a) The initial neutron energy spectrum of source, (b) the simulation result of neutron dose rate, (c) the simulation result of second photon dose rate, (d) the second photon dose spectrum of 8-cm-thick PPNM–20% B_4C, PPNM–0% B_4C, and PE/PEW.

thickness of shield was less than 16 cm, the photon dose rate of PPNM increases with the increase of B_4C content. However, the opposite result occurs after 16 cm. These are the results of balance between photon generation and attenuation.

When the thickness of the shield was less than 6 cm, the dose of the photon rate of PE/PEW was smallest compared with that of all other composites, but the photon dose rate increased faster than that of PPNMs containing B_4C and exceeded then after 6 cm. For neutron shielding, the photon dose rate possesses a more meaningful value when the neutron has almost been entirely shielded. The PPNMs containing B_4C have better secondary gamma-ray shielding ability than PE/PEW. The photon dose curves of PPNM–0% B_4C were always kept higher than that of PE/PEW. It means that gamma-rays generated in PPNM–0% B_4C were more than that in PE/PEW because of the nickel foams. However, the photon dose rate of PPNM–20% B_4C was lower than that of PE/PEW–20% B_4C when the thickness of the shield was over 16 cm. Thus, the nickel foams in PPNM–20% B_4C and PPNM–0% B_4C played different roles in generating secondary gamma-rays. To explain this, the second photon dose spectrum of 8-cm-thick PPNM–20% B_4C, PPNM–0% B_4C, and PE/PEW is shown in Figure 8(d). The energy of the secondary gamma-rays and the reaction cross-section were changed with different materials and neutron energy. For PE/PEW, the highest peak appeared between 2 and 3 MeV. The energy of most gamma-rays which come from capture reaction is 2.224 MeV. Therefore, H was the main neutron-absorbing element in PE/PEW. For PPNM–0%, the line with square points in Figure 8 shows that the energy of the gamma-ray comes from capture reaction between Ni and the neutron is much higher than that of H, and these gamma rays cause a high-dose rate in the detector. For PPNM–20% B_4C, the highest peak appeared in 0.48 MeV ($^{10}B + n \rightarrow Li + {}^4He + \gamma + 0.48$ MeV); thus, B absorbed most of the thermal neutron. At the same time, the 3D network of the Ni foams can absorb more photons than PE/PEW; therefore, the photon dose rate of PPNM–20% could be lower than PE/PEW–20% B_4C when the thickness of the shield was greater than 16 cm.

Conclusion

A new PPNM neutron-shielding material with different content of B_4C was fabricated by infusing the melting mixture of fillers into open-cell nickel foams. The viscosity of melting fillers with different proportions of PE and PEW were investigated to improve the filling rate of composite. The OM and SEM were used to observe the morphological characteristics of the section and fracture surface. The compression responses and thermal conductivity of PPNM and PE/PEW were studied. The neutron-shielding ability and secondary gamma-rays were studied by the Monte Carlo particle transport simulation. The major conclusions of this work are as follows:

1. The PPNMs which filled with the mixture of PE and PEW in the ratio of 1:1 had high filling rate. SEM and OM photographs showed that the B_4C particles with surface treatment were well dispersed in the matrix and interfacial bonding between B_4C and PE/PEW was reinforced.
2. The 3D metal network of nickel foams improved thermal conductivity of PE/PEW by 300%.
3. The compression strength of PPNMs containing B_4C was almost equivalent to that of PE/PEW. The compression strength increased with the mass fraction of B_4C from 0% to 20%, and slightly decreased from 20% to 40%. The energy-absorbed efficiency of PPNMs was improved 30% compared with PE/PEW.
4. The calculated results showed that the neutron shield ability of PPNM–0% B_4C was almost the same as that of PE/PEW, it is influenced less by the nickel foams. The neutron shield ability of PPNMs increased with increasing of the mass fraction of B_4C. Under the condition of 29 cm shield, the permeable neutron dose rate of PPNM–10% B_4C, PPNM–20% B_4C, PPNM–30% B_4C, and PPNM–40% B_4C was about 22.9%, 41.1%, 52.1%, and 58.3% lower than that of PE/PEW, respectively.
5. Under the condition of 29 cm shield, the secondary gamma-ray shielding ability of PE/PEW and PPNM–0% B_4C were much lower than other PPNMs with B_4C. The percentage decrease in the secondary gamma-ray dose rate of PPNMs with B_4C with respect to PE/PEW was approximately 84–89%.

Authors' Note

Feida Chen contributed equally to this work and should be considered co-first authors.

Declaration of conflicting interests

The author(s) declared no potential conflicts of interest with respect to the research, authorship, and/or publication of this article.

Funding

The author(s) disclosed receipt of the following financial support for the research, authorship and/or publication of this article: This work was supported by the Fundamental Research Funds for the Central Universities (Grant No. NJ20150021), the National Key Research and Development Program (Grant No. 2016YFE0103600), and the Foundation

of Graduate Innovation Center in NUAA (Grant No. kfjj20160604, Grant No. kfjj20170609). This work was supported by the Priority Academic Program Development of Jiangsu Higher Education Institutions.

References

1. Zhang P, Li Y, Wang W, et al. The design, fabrication and properties of B4C/Al neutron absorbers. *J Nucl Mater* 2013; 437: 350–358.
2. Lee MK, Lee JK, Kim JW, et al. Properties of B4C–PbO–Al(OH)(3)–epoxy nanocomposite prepared by ultrasonic dispersion approach for high temperature neutron shields. *J Nucl Mater* 2014; 445: 63–71.
3. Moon J and Yi S. Mechanical properties and thermal neutron shielding efficiency of high B amorphous ribbons in the Fe–B–Mo–Cr system. *Met Mater Int* 2016; 22: 825–830.
4. Ozdemir T, Akbay IK, Uzun H, et al. Neutron shielding of EPDM rubber with boric acid: mechanical, thermal properties and neutron absorption tests. *Prog Nucl Energy* 2016; 89: 102–109.
5. Yadollahi A, Nazemi E, Zolfaghari A, et al. Optimization of thermal neutron shield concrete mixture using artificial neural network. *Nucl Eng Des* 2016; 305: 146–155.
6. Chen W, Wang J, Wang T, et al. Electromagnetic interference shielding properties of nickel-coated carbon fiber veil/acid-functionalized MWCNTs/epoxy multiscale composites. *J Reinf Plast Compos* 2015; 34: 1029–1039.
7. Wang G, Cao D, Yin C, et al. Nickel foam supported-Co3O4 nanowire arrays for H_2O_2 electroreduction. *Chem Mater* 2009; 21: 5112–5118.
8. Akkas A, Tugrul AB, Buyuk B, et al. Shielding effect of boron carbide aluminium metal matrix composite against gamma and neutron radiation. *Acta Phys Pol A* 2015; 128: B176–B9.
9. Huang Y, Zhang W, Liang L, et al. A "Sandwich" type of neutron shielding composite filled with boron carbide reinforced by carbon fiber. *Chem Eng J* 2013; 220: 143–150.
10. Chen S, Bourham M and Rabiei A. Attenuation efficiency of X-ray and comparison to gamma ray and neutrons in composite metal foams. *Radiat Phys Chem* 2015; 117: 12–22.
11. Kaewjang S, Maghanemi U, Kothan S, et al. New gadolinium based glasses for gamma-rays shielding materials. *Nucl Eng Des* 2014; 280: 21–26.
12. Shin JW, Lee J-W, Yu S, et al. Polyethylene/boron-containing composites for radiation shielding. *Thermochim Acta* 2014; 585: 5–9.
13. Yu H, Tang X, Wang P, et al. Safety verification of radiation shielding and heat transfer for a model for dry. *Nucl Eng Des* 2015; 291: 287–294.
14. Saiyad M, Devashrayee NM and Mevada RK. Study the effect of dispersion of filler in polymer composite for radiation shielding. *Polym Compos* 2014; 35: 1263–1266.
15. Gwaily SE, Hassan HH, Badawy MM, et al. Study of electrophysical characteristics of lead-natural rubber composites as radiation shields. *Polym Compos* 2002; 23: 1068–1075.
16. Yuan J, Chen X, Zhou W, et al. Study on quasi-static compressive properties of aluminum foam-epoxy resin composite structures. *Compos B Eng* 2015; 79: 301–310.
17. Xiao X, Zhang P and Li M. Preparation and thermal characterization of paraffin/metal foam composite phase change material. *Appl Energy* 2013; 112: 1357–1366.
18. Ji K, Xia Y and Dai Z. Different foamed metal-reinforced composites: tribological behavior and temperature field simulation. *Tribol T* 2013; 56: 615–622.
19. Peroni M, Solomos G and Pizzinato V. Impact behaviour testing of aluminium foam. *Inter J Impact Eng* 2013; 53: 74–83.
20. Xiong X, Ding D, Chen D, et al. Three-dimensional ultrathin Ni(OH)(2) nanosheets grown on nickel foam for high-performance supercapacitors. *Nano Energy* 2015; 11: 154–161.
21. Jung A and Diebels S. Synthesis and mechanical properties of novel Ni/PU hybrid foams: a new economic composite material for energy absorbers. *Adv Eng Mater* 2016; 18: 532–541.
22. Xu SQ, Bourham M and Rabiei A. A novel ultra-light structure for radiation shielding. *Mater Des* 2010; 31: 2140–2146.
23. Chen S, Bourham M and Rabiei A. Neutrons attenuation on composite metal foams and hybrid open-cell Al foam. *Radiat Phys Chem* 2015; 109: 27–39.
24. Gong XL, Liu Y, He SY, et al. Manufacturing and low-velocity impact response of a new composite material: metal porous polymer composite (MPPC). *J Mater Sci Technol* 2004; 20: 65–68.
25. Fan L-W and Jin H-Q. Local thermal nonequilibrium during melting of a paraffin filled in an open-cell copper foam: a visualized study at the pore-scale. *J Heat Trans-T ASME* 2017; 139.
26. Babaei M, Sadighzadeh A, Kiashemshaki M, et al. Simulation and design of biological shield for the 115 kJ IR-MPF-100 plasma focus device using MCNP code. *J Fusion Energy* 2016; 35: 579–584.
27. Soltani Z, Beigzadeh A, Ziaie F, et al. Effect of particle size and percentages of boron carbide on the thermal neutron radiation shielding properties of HDPE/B4C composite: experimental and simulation studies. *Radiat Phys Chem* 2016; 127: 182–187.
28. Zhang Y, Chen F, Tang X, et al. Preparation and characterization of paraffin/nickel foam composites as neutron-shielding materials. *J Compos Mater*. DOI: 10.1177/0021998317717596.
29. Wang X, Ma Y, Liu W, et al. Mode I interfacial fracture characterization of foam core sandwich materials at elevated temperatures. *J Reinf Plast Comp* 2017; 36: 1009–1018.
30. Chen C, Li Y, Gu Y, et al. Improvement in skin-core adhesion of multiwalled carbon nanotubes modified carbon fiber prepreg/Nomex honeycomb sandwich composites. *J Reinf Plast Comp* 2017; 36: 608–618.
31. Papadopoulos DP and Konstantinidis IC. Mechanical properties of Al metal foams. *Mater Lett* 2004; 58: 2574–2578.